Cell Reports Medicine, Volume *5*

Supplemental information

Genetic and microenvironmental evolution of colorectal liver metastases under chemotherapy

Min Shi, Yingxi Yang, Na Huang, Dongqiang Zeng, Zongchao Mo, Jiao Wang, Xiaomeng Zhang, Ran Liu, Chunlin Wang, Xiaoxiang Rong, Zhenzhen Wu, Qiong Huang, Haixia Shang, Jihong Tang, Zhaojun Wang, Jianan Cai, Genjie Huang, Yijin Guan, Jian Guo, Quanhua Mu, Jiguang Wang, and Wangjun Liao

A Baseline patient characteristics according to response status of first-line therapy

	Total (n=48)	R (n=27)	NR (n=21)	p-Value
Age at enrollment (years)				
Median (range)	55.5 (29-79)	57.4 (33-73)	53.1 (29-79)	0.33[a]
Sex (n (%))				
Female	20 (42)	10 (37)	10 (48)	0.56[b]
Male	28 (58)	17 (63)	11 (52)	
Stage (n (%))				
IVA	17 (35)	7 (26)	10 (48)	0.14[b]
IVB	23 (48)	16 (59)	7 (33)	0.09[b]
IVC	8 (17)	4 (15)	4 (19)	0.72[b]
Primary tumor site (n (%))				
Left	37 (77)	19 (70)	18 (86)	0.30[b]
Right	11 (23)	8 (30)	3 (14)	
Smoking history (n (%))				
Yes	10 (21)	7 (26)	3 (14)	0.48[b]
No	38 (79)	20 (74)	18 (86)	
Alcohol drinking history (n (%))				
Yes	4 (8)	2 (7)	2 (10)	1.00[b]
No	44 (92)	25 (93)	19 (90)	
Lung metastases (n (%))				
Yes	20 (42)	15 (56)	5 (24)	0.04[b]
No	28 (58)	12 (44)	16 (76)	
Number of metastases (n (%))				
1 (liver-only)	16 (33)	6 (22)	10 (48)	0.12[b]
>=2	32 (38)	21 (78)	11 (52)	
First-line therapy (n (%))				
BVZ+mFOLFOX6	35 (73)	21 (78)	14 (67)	0.52[b]
BVZ+FOLFIRI	13 (27)	6 (22)	7 (33)	

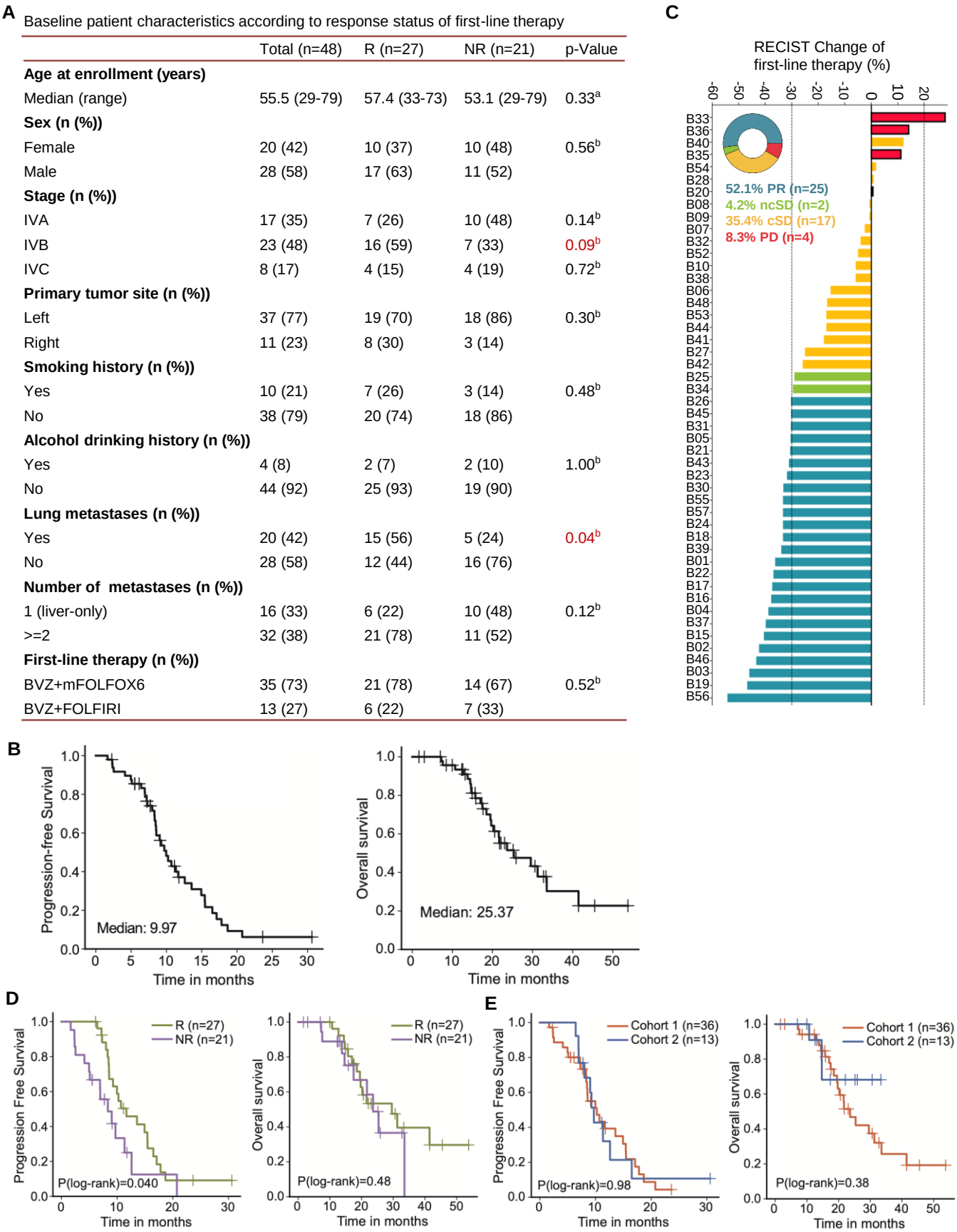

Figure S1. Clinical information of the enrolled CRLM patients, related to Figure 1.

(**A**) Relationship between baseline patient characteristics and their response status to first-line therapy. P-values were calculated by either Mann-Whitney U test (labelled with "a") or two-sided Fisher's exact test (labelled with "b"). (**B**) Kaplan–Meier estimates of progression-free survival (left panel) and overall survival (right panel) for all enrolled patients. (**C**) Waterfall plot demonstrating best percentage reduction of tumor burden with the guideline (Figure 1C) for first-line therapy. The vertical dotted line represented the threshold of 30% regression and 20% progression in tumor size. Patients with new lesions were highlighted with black border. (**D**) Kaplan–Meier estimates of progression-free survival (left panel) and overall survival (right panel) for first-line Responders (R) and Non-responders (NR). (**E**) Kaplan–Meier estimates of progression-free survival (left panel) and overall survival (right panel) as per treatment arm.

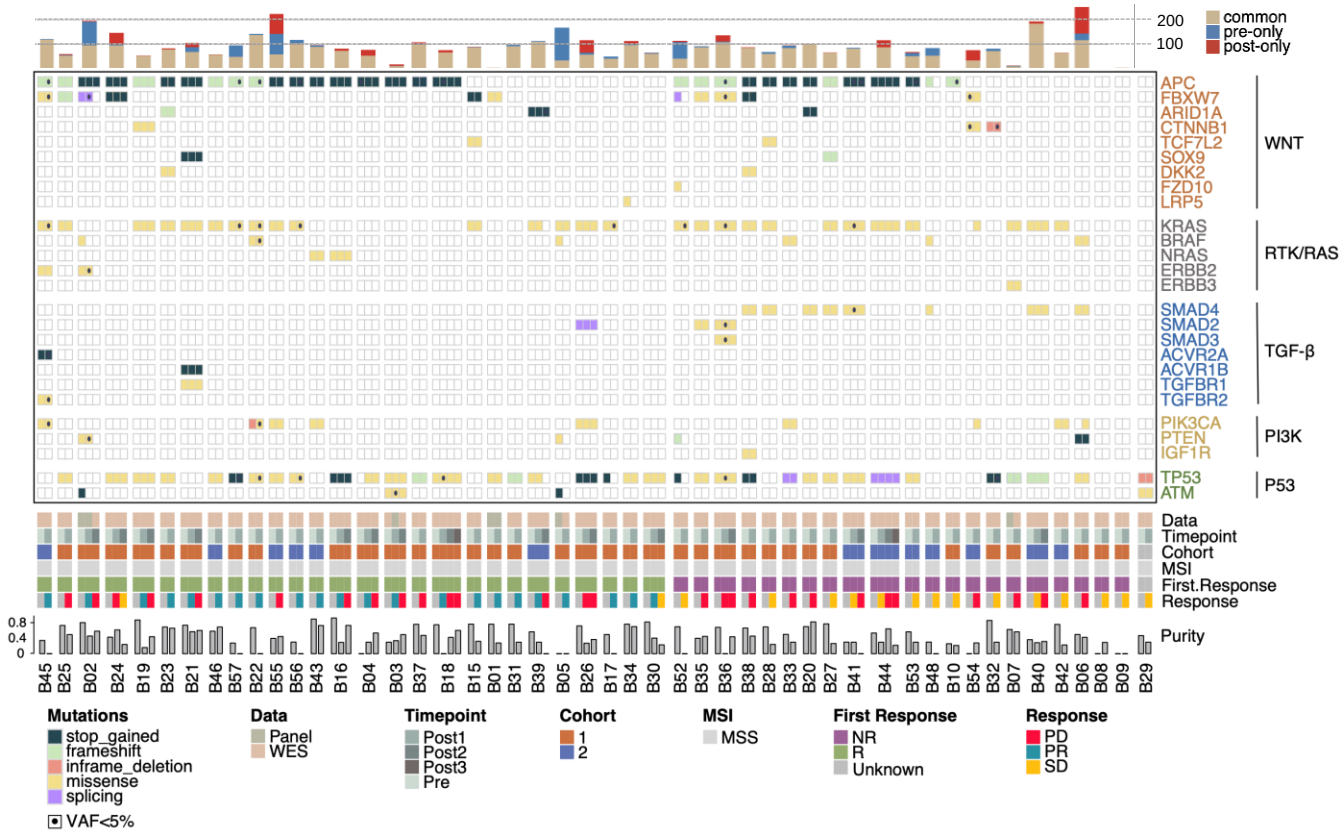

Figure S2. Somatic mutational landscape of pre- and post-treatment CRLM tumors, related to Figure 2.
Nonsynonymous mutations in 115 matched diagnostic and treated tumor samples. The top panel demonstrated the number of somatic mutations that are shared (common), pre-treatment private or post-treatment private. The middle panel included somatic mutations of known CRC driver genes that were clustered by pathway. The third panel annotated each sample by WES/panel, pre-/post-treatment, MSI status, response status of first-line therapy and timepoint response. Each column represents a sample and patients were ordered by first-line response. Purity (estimated by Facets) of each tumor sample was showed at the bottom panel. MSS. microsatellite stable.

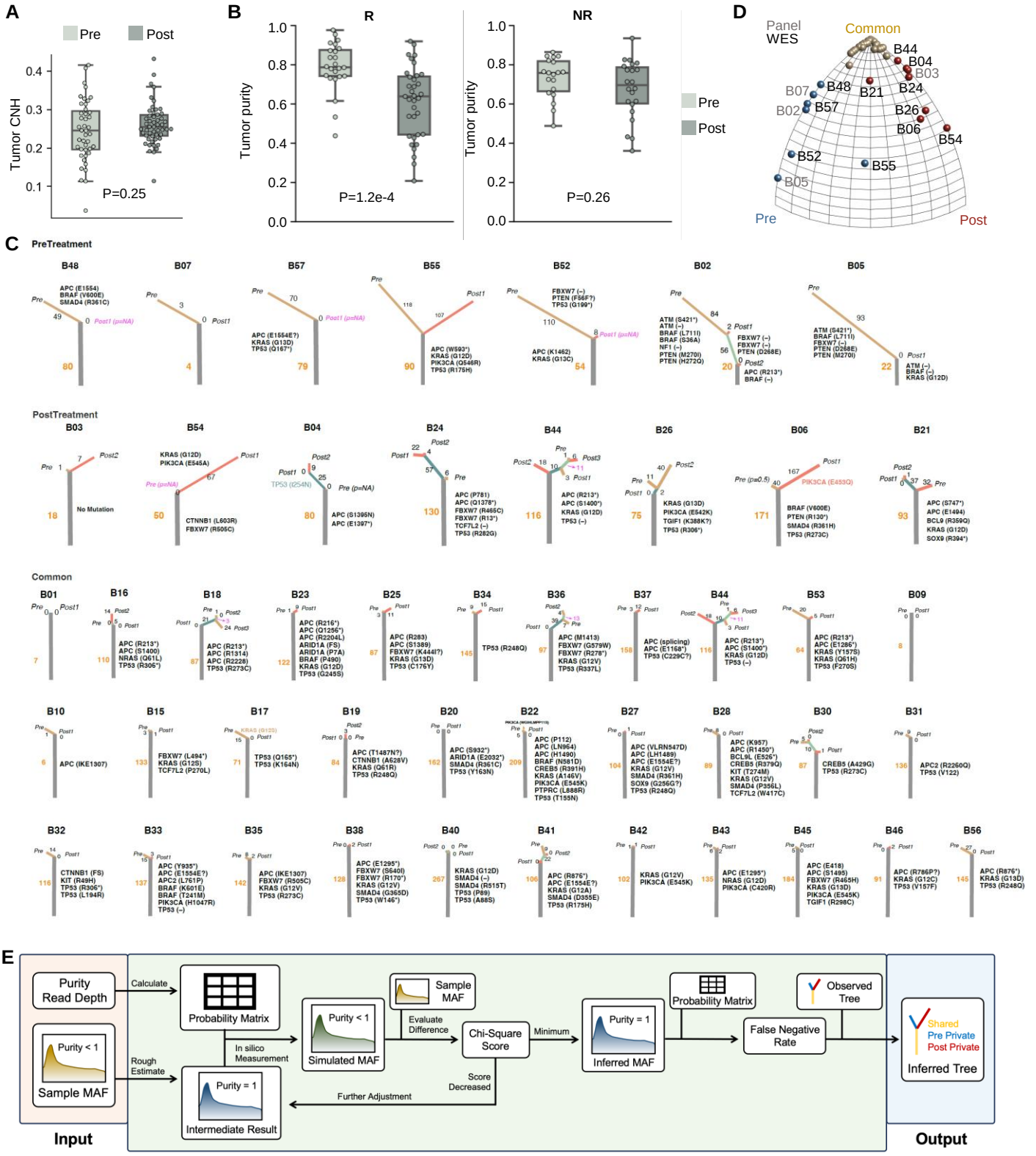

Figure S3. CLRM evolution under BVZ-based chemotherapy, related to Figure 2.
(**A**) Chromosomal copy number heterogeneity (CNH) of pre-treatment tumors versus post-treatment tumors. P-value was calculated by Mann-Whitney U test**.** (**B**) Comparison of tumor purity in the treatment-responsive group (left) and the non-responsive group (right) before and after treatment. P values were determined by the Mann-Whitney U test. (**C**) Phylogenetic trees of 49 CLRM patients based on genomic sequencing of their matched pre- and post-treatment tumor samples. (**D**) Moduli space of evolutionary trees before ETRIP adjustment. (**E**) Overview workflow of ETRIP pipeline (see details in STAR Methods).

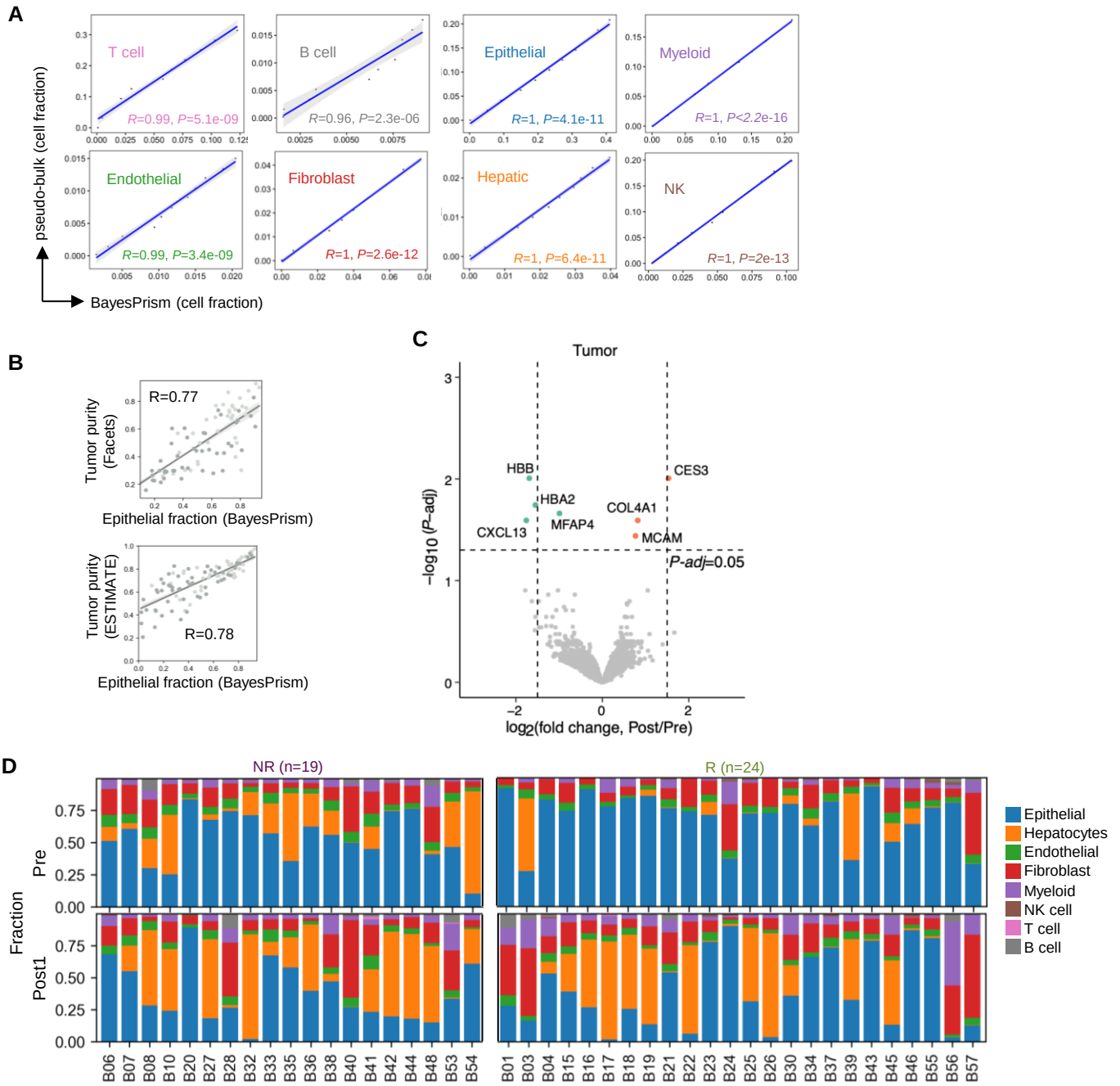

Figure S4. Tumor microenvironment profile calculated by BayesPrism, related to Figure 3.
(**A**) Scatter plots showing the correlation between the ground truth and the BayesPrism-inferred proportion for each cell type. Gene expression profiles were obtained from synthetic mixtures composed of diverse combinations of single cells. (**B**) Scatter plots showing the correlation between the tumor purity and epithelial cell fraction inferred by BayesPrism. The tumor purity was inferred by Facets with DNA-seq (left panel) or ESTIMATE with RNA-seq (right panel). (**C**) Volcano plot showing DEGs in post-treatment tumors versus pre-treatment tumors. The tumor gene expression was estimated by BayesPrism and differential gene expression was analyzed using DESeq2. (**D**) The cell type composition of each sample with pre-treatment (Pre) on the top and post-treatment (Post1) on the bottom.

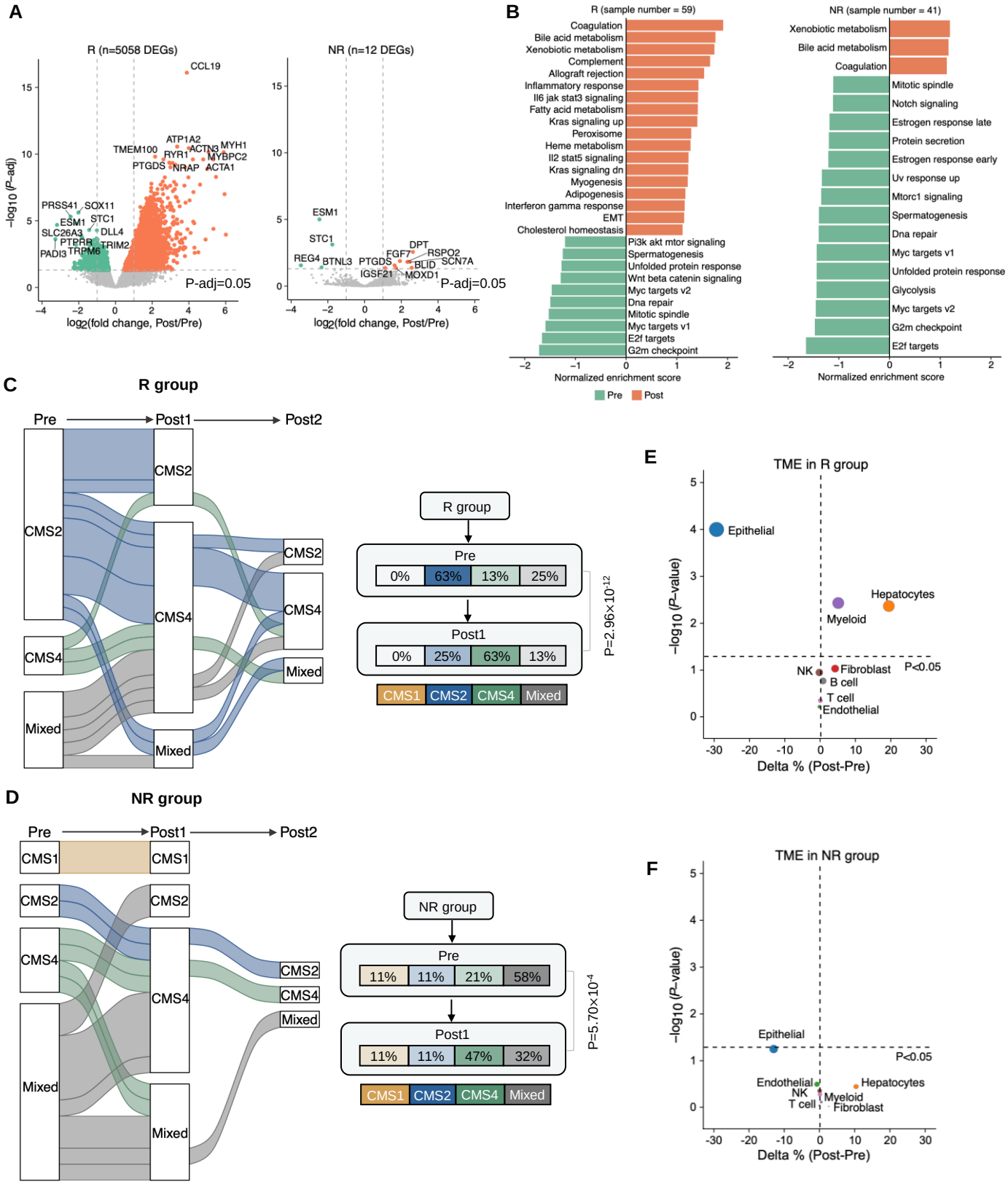

Figure S5. Transcriptional changes before and after treatment by the response group, related to Figure 3.

(**A**) Volcano plot showing DEGs in post-treatment versus pre-treatment tumor samples in responder (left) and non-responder (right) group. The log2 foldchanges were extracted from DESeq2 and P-value: the Wald test. P values were then adjusted for multiple testing using the Benjamini-Hochberg procedure (P-adj). Significantly DEGs with P-adj < 0.05 were colored and selected top genes were labelled. (**B**) GSEA showing the enriched pathways in baseline compared with post-treatment samples in responder (left) and non-responder (right) group. (**C**-**D**) Alluvial plot showing CMS transition under treatment (left panel) in responder (C) and non-responder (D) group. The right panel displayed the change of proportion in each subtype. P-value: Chi-squared test. (**E**-**F**) Bubble plot demonstrating the percentage changes of various cell types between post-treatment and pre-treatment samples in responder (E) and non-responder (F) group. The relative percentage of each cell type within the bulk RNA-seq samples was inferred by the deconvolution method BayesPrism, with the public CRLM scRNA-seq data (dbGAP: phs001818.v3.p1) as a reference. The change in percentage (Delta %) was calculated by subtracting the average cell type proportions in treated samples from those in baseline samples. The bubble size was proportional to -log10(P-value). P-value: Mann–Whitney U-test.

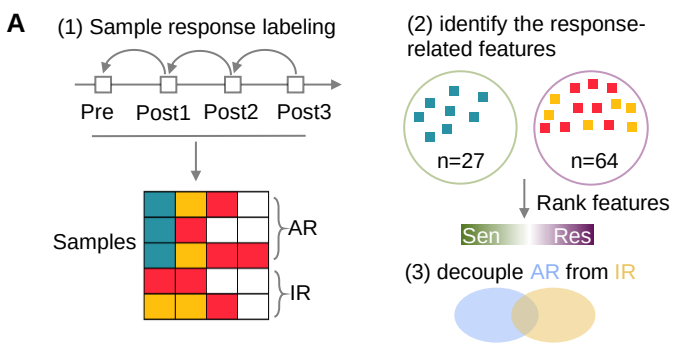

B

AR	Res	Sen
DNA mutation	0	0
Mutation burden	0	0
CNA	0	0
CNH	0	0
Tumor purity	0	1
RNA gene expression	80	20
CMS subtypes	1	1
Cell type proportion	2	2

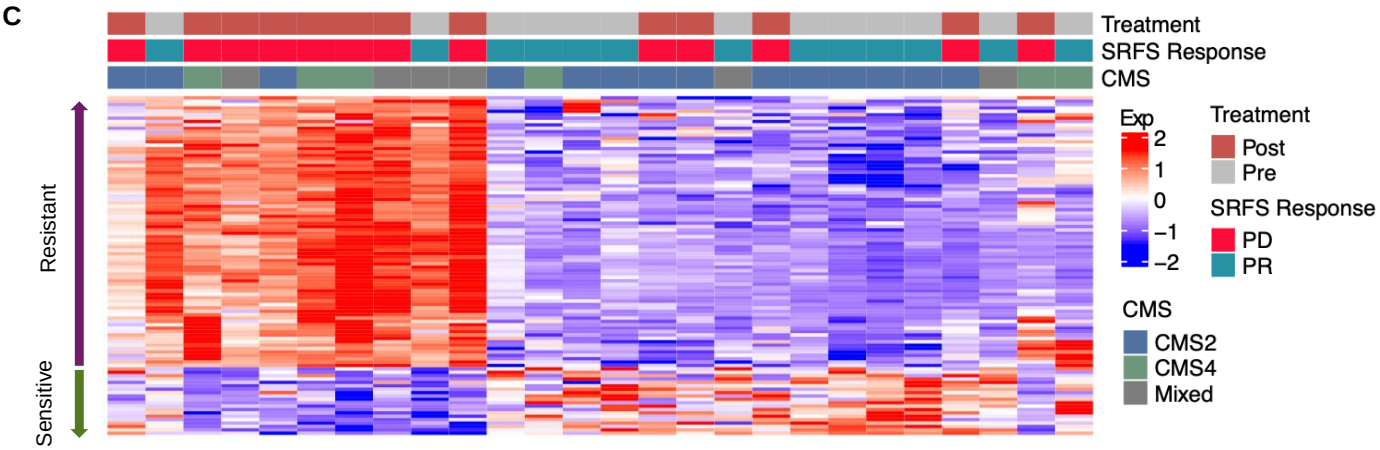

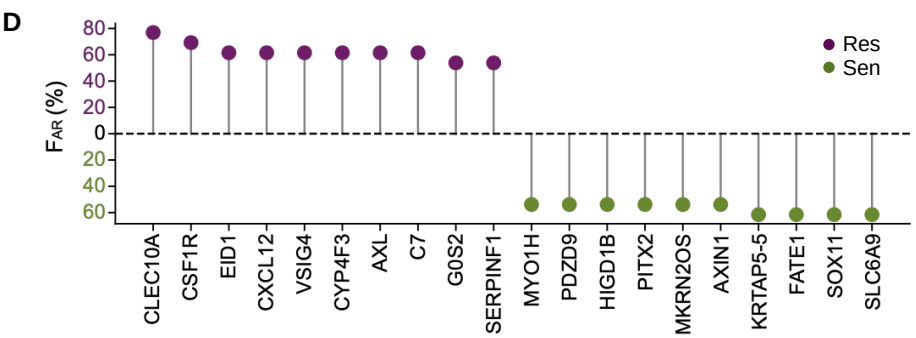

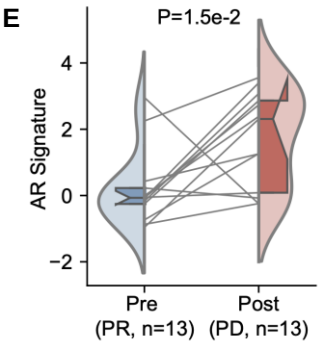

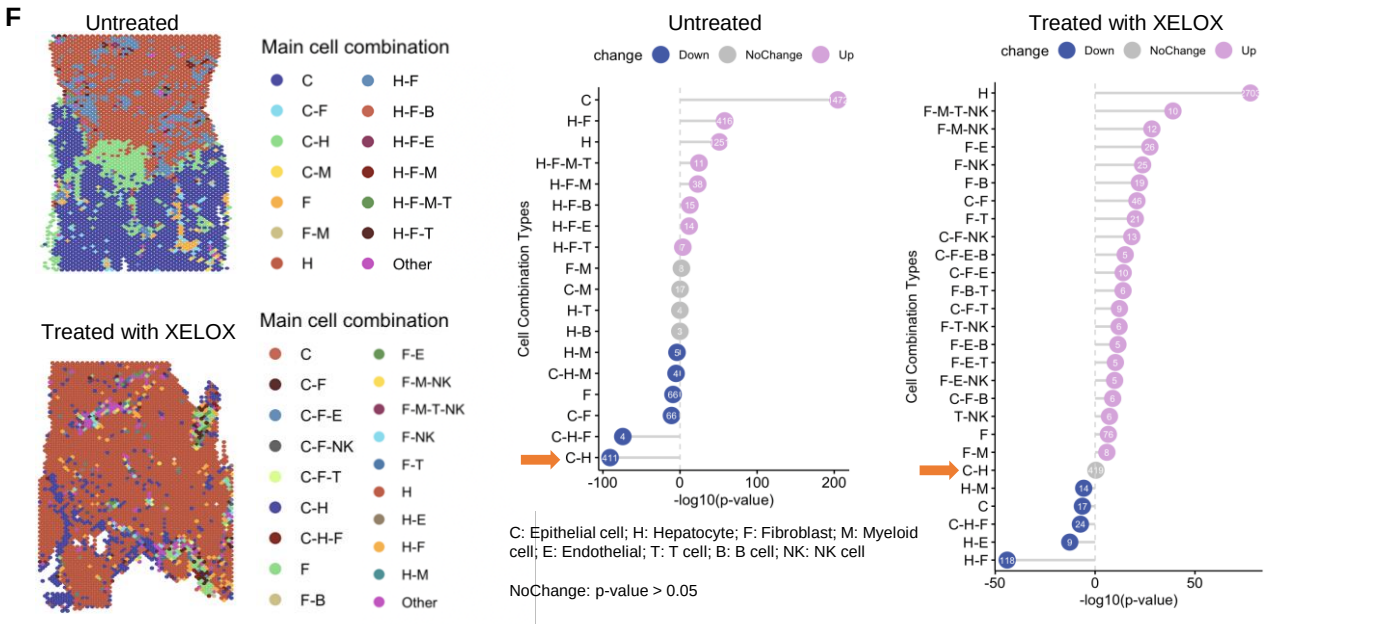

Figure S6. Transcriptomic analysis of sensitive versus resistant samples under treatment, related to Figure 3.
(**A**) Overview of the Sample-based Response Feature Selection (SRFS) approach for identifying treatment response-related factors. Step 1: pooling samples, and re-annotating the sample responses based on their future response labels. Step 2: categorizing samples into sensitive (PR) or resistant (SD or PD) groups, evaluating genomic and transcriptomic features for discriminative potential, and classifying them as resistance (Res)- or sensitivity (Sen)-related. Step 3: decoupling AR and IR features based on the IR and AR contribution thresholds (see STAR Methods). (**B**) Statistics of AR-related features identified by SRFS. (**C**) Heatmap showing the expression of AR-related genes from 13 patients with baseline (PR, n=13) and matched treated recurrent samples (PD, n=13). (**D**) Lollipop plot showing the top 10 genes related to AR. The y-axis represents the fraction of patients whose AR was potentially contributed by certain gene expression. (**E**) Comparisons of AR signatures (see Methods) between pre-treatment PR samples and matched post-treatment PD samples in 13 patients. This analysis focused on patients who initially showed a PR but later progressed to PD. P value: two-sided paired t-test. (**F**) Spatial distribution of different cell types within a pre-treatment sample (left top panel) and a sample after treatment (left bottom panel). Lollipop plots showed spatial interactions or spatial exclusion of cell type combinations before (middle panel) and after (right panel) therapy. The number in dots represented number of spots harboring the cell type combination. The color of the dots indicated whether spots with the cell type combination were significantly enriched in the sample with red representing significantly enriched, blue representing significantly depleted, and grey representing not significant (p-value > 0.05).

A

IR	Res	Sen
DNA mutation	2	0
Mutation burden	0	0
CNA	0	4
CNH	0	0
Tumor purity	0	1
RNA gene expression	47	42
CMS subtype	0	1
Cell type proportion	1	2

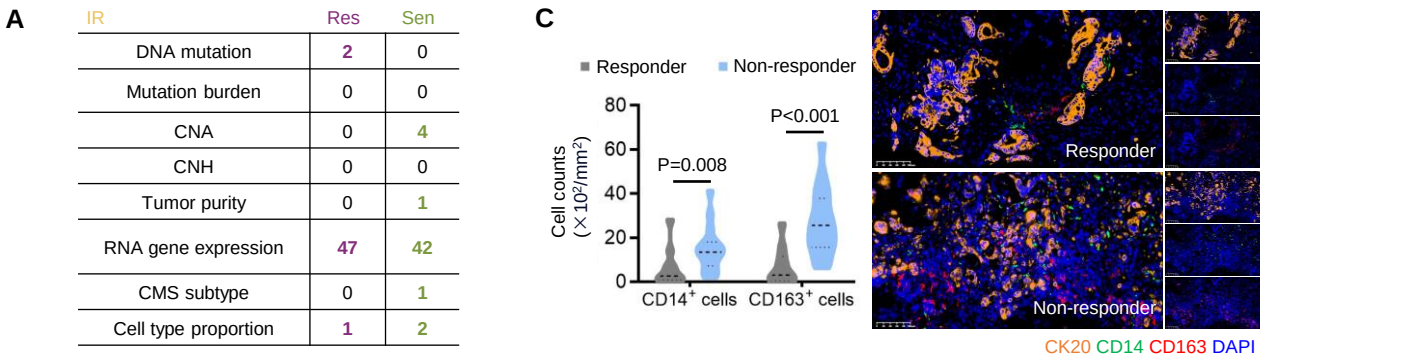

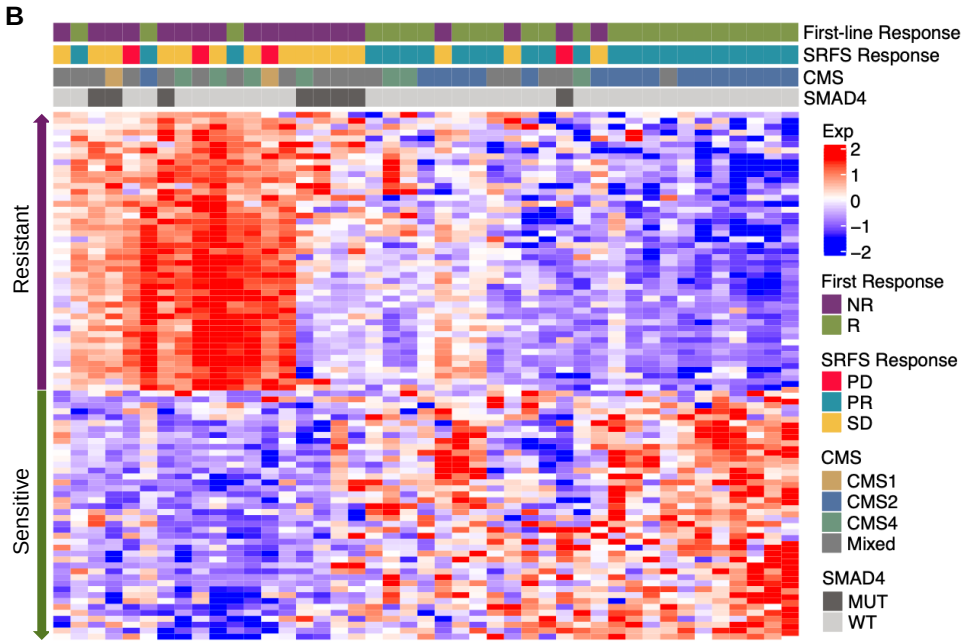

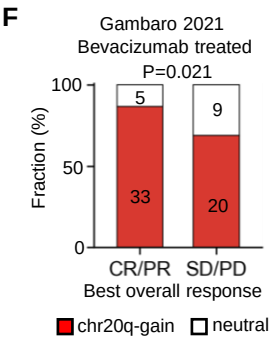

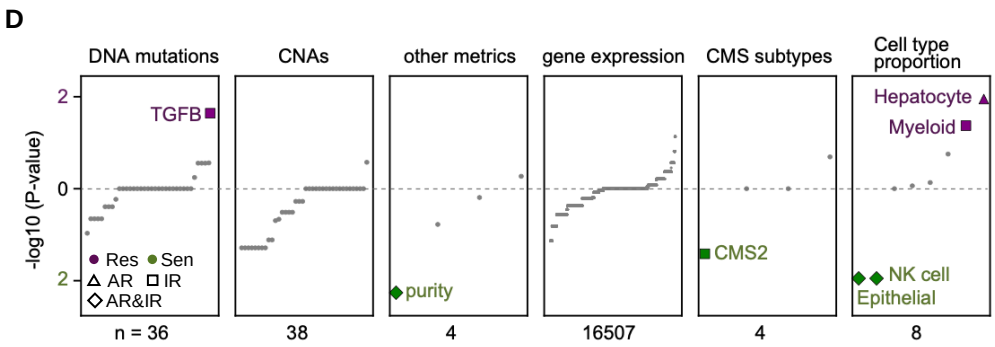

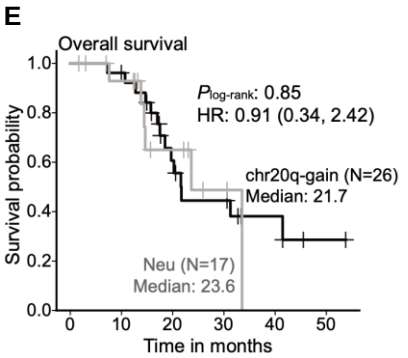

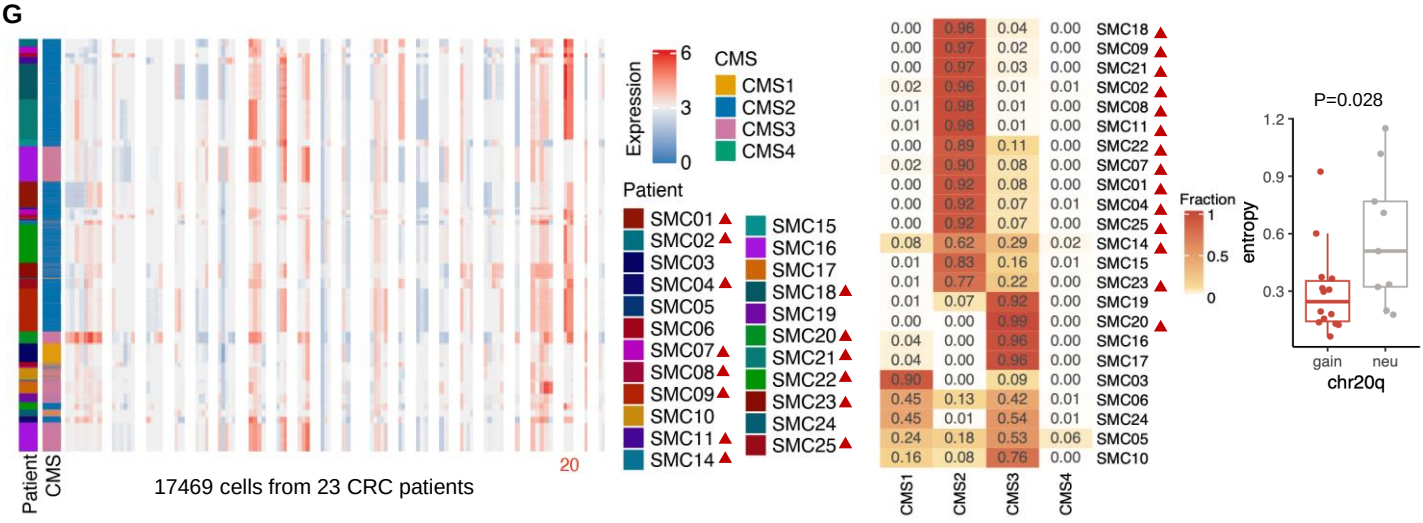

Figure S7. chr20q gain were associated with IR, related to Figure 4.
(**A**) Statistics of the detected AR-related feature by SRFS. (**B**) Heatmap showing the expression profile of IR-related genes in pre-treatment tumor samples. (**C**) Quantification (left) and representative IF images (right) of monocytes (CD14+) and macrophages (CD163+) in hepatic metastasis samples from responders (n = 10) and non-responders (n = 17). P value: Mann-Whitney U test. Scale bars = 100 μm. (**D**) Different types of features prioritized by SRFS in patients with RHGP. Each dot represented an individual feature and significant AR or IR-associated features were highlighted in green (pro-sensitive) or purple (pro-resistant). (**E**) Kaplan–Meier estimates of overall survival for patients segregated by chr20q-gain. (**F**) Chr20q gain was associated with response to BVZ-based therapy in an independent cohort reported by *Gambaro 2021*. CR: complete response. P value: exact binomial test. Pre-treatment CRLM patients treated with Oxaliplatin, Irinotecan or Oxaliplatin + Irinotecan + BVZ were included. (**G**) Representative CNV heatmaps (left) from inferCNV analysis from tumor cells in CRC patients (GSE132465). The patients with chr20q gain were labelled by a red triangle. Each single cell was annotated with a CMS subtype determined by the highest similarity scores of each tumor cell to the reference CMS gene expression programs (*Guinney J 2015*). CMS distribution in each patient (middle). Comparison of the entropy scores in chr20q-gain versus chr20q-neutral patients (right). Lower entropy values indicated a more stable cellular state. P value: Mann-Whitney U test.

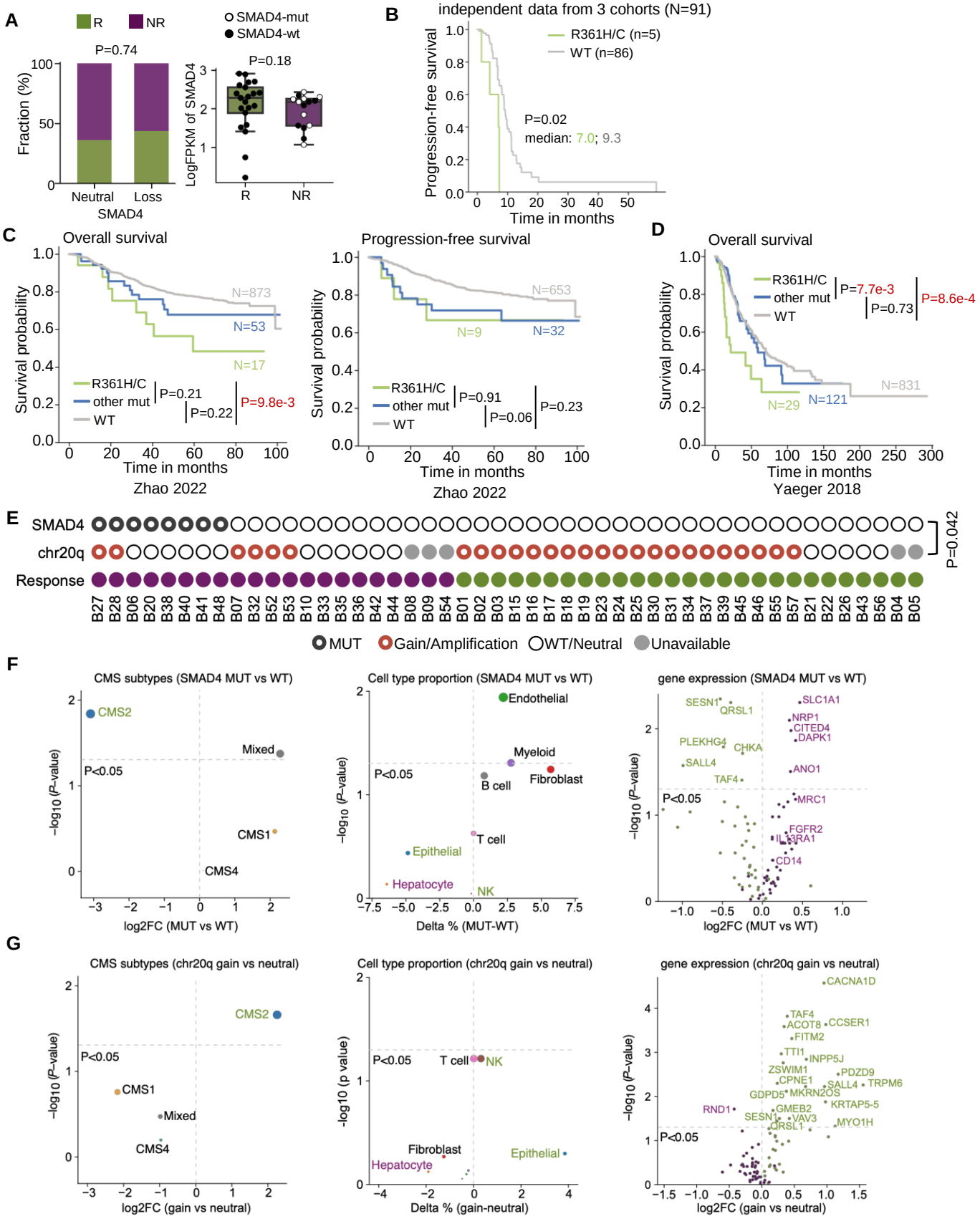

Figure S8. *SMAD4* mutations was associated with IR, related to Figure 4.

(**A**) Bar plot (left) comparing the non-responding frequency in SMAD4 copy number loss and neutral groups before treatment. P-value was calculated by one-proportion z-test. Box plot (right) showed the expression level of SMAD4 for pre-treatment samples from either responders or non-responders. P-value: Mann-Whitney U test. (**B**) Kaplan–Meier estimates of progression-free survival in the independent Chinese cohorts segregated by SMAD4$^{R361H/C}$ mutation status defined by ddPCR. (**C**) Kaplan–Meier estimates of overall survival (left panel) and progression-free survival (right panel) in another independent cohort, Chinese ChangKang CRC cohort stratified by SMAD4 mutation status. Patients diagnosed with pathological stage IV were included, irrespective of their treatment status. (**D**) Kaplan–Meier estimates of overall survival in MSK CRC cohort stratified by SMAD4 mutation status. All patients were included, irrespective of their treatment status. (**E**) Exclusivity between SMAD4 mutations and gain of chr20q. P-value was calculated by two-sided Fisher's exact test. (**F-G**) CMS subtype distribution (left), relative percentage of cell types (middle), and the expression of IR-related genes (right) in SMAD4-mutant versus SMAD4-wildtype samples (F), as well as chr20q-gain versus chr20q-neutral samples (G) prior to treatment. Each dot represented an individual feature and the IR-associated features were highlighted in green (pro-sensitive) or purple (pro-resistant) detected by our method SRFS. P values: two-sided Fisher exact test (left) and Mann-Whitney U test (middle and right), respectively.

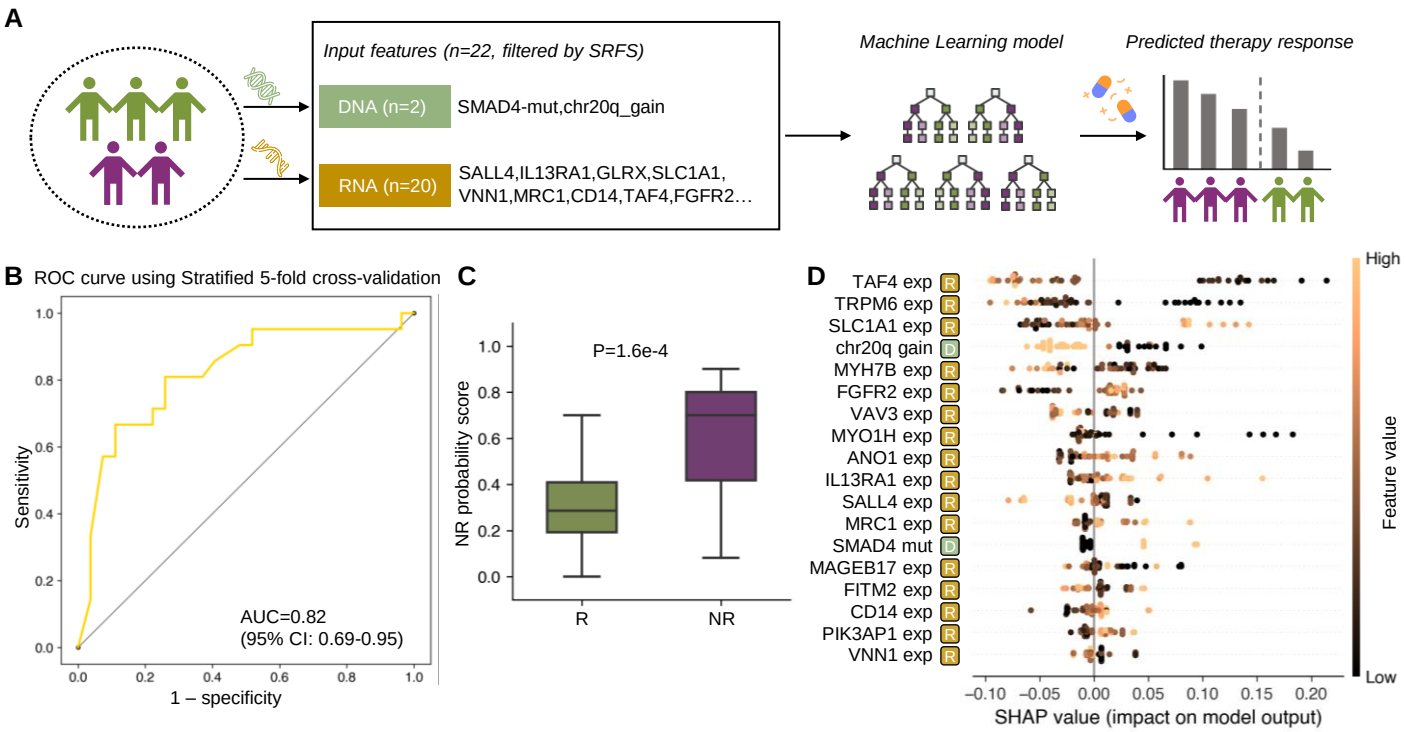

Figure S9. Machine learning model designed for the early prediction of drug resistance or sensitivity in CRLM patients, related to Figure 4.

(**A**) Schematic illustration of machine learning model to predict BVZ-C therapy responders and non-responders. Input features (n=22) included the IR-related features (DNA: SMAD4 mutation and chr20q gain; RNA: top ten pro-sensitive and pro-resistant genes) selected by SRFS. Bayesian ridge were used for imputation of missing data in 48 CRLM pretreatment samples and a 22-feature prognositic model (Random Forest) was trained with hyperparameters optimization. (**B**) Receiver operating characteristic (ROC) curves showing the model performance in stratified 5-fold cross-validation. (**C**) Model probability score distributions in responder and non-repsonder samples. P value was determined by Mann-Whitney U test. (**D**) Shapley additive explanation (SHAP) value of each feature in the model.

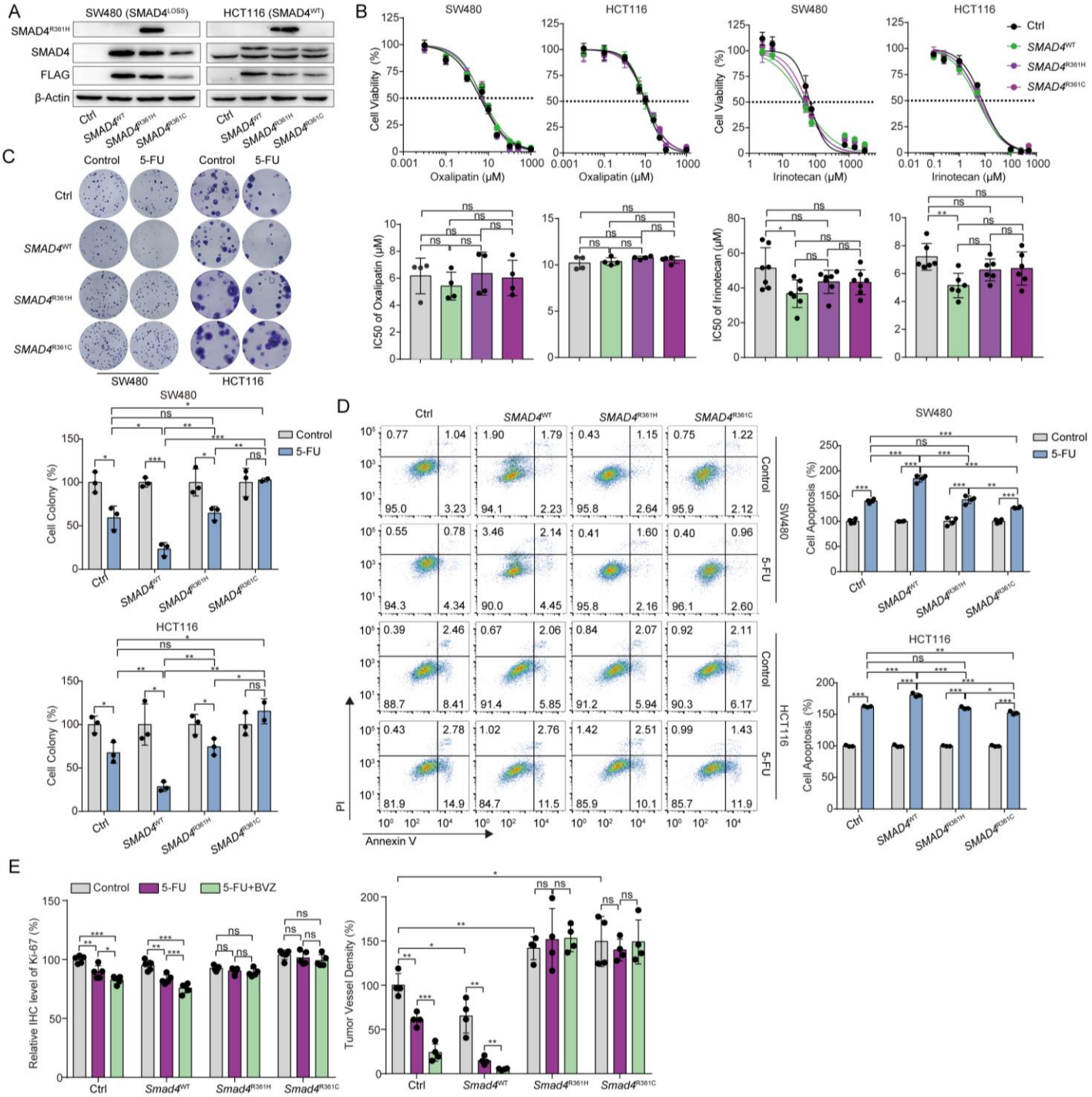

FigureS10. *SMAD4*$^{R361H/C}$mutationspromote5-FUandbevacizumabresistanceinCRC, related to Figure 5.
(A) Western blotting confirming ectopic expression of SMAD4, SMAD4$^{R361H/C}$, and FLAG in retrovirally transduced SW480 and HCT116 cells. **(B)** Cell viability assay of SW480 and HCT116 cells following treatment with Oxaliplatin or Irinotecan for 48 hours, IC50 value of Oxaliplatin or Irinotecan (bottom) and representative curve-fitting graphs (top) are shown (n=4,6). **(C)** Colony formation assay and the quantitative graph of SW480 and HCT116 cells exposed to 5-FU for two weeks. Representative images (top) and the quantification (bottom) of the numbers of colonies are shown (n=3). **(D)** Flow cytometry of apoptosis and the quantitative graph of SW480 and HCT116 cells following treatment to 5-FU for 48h (n=3,4). **(E)** Transplanted subcutaneous tumors with treatment are collected, and the quantification for immunohistochemical (IHC) staining of tumor-proliferation marker Ki-67 and immunofluorescence of tumor vascular markers CD31 are shown (n=4,5). Data are graphed as the mean ± SD; *, P < 0.05; **, P < 0.01; ***, P < 0.001; ns, nonsignificant, P > 0.05.

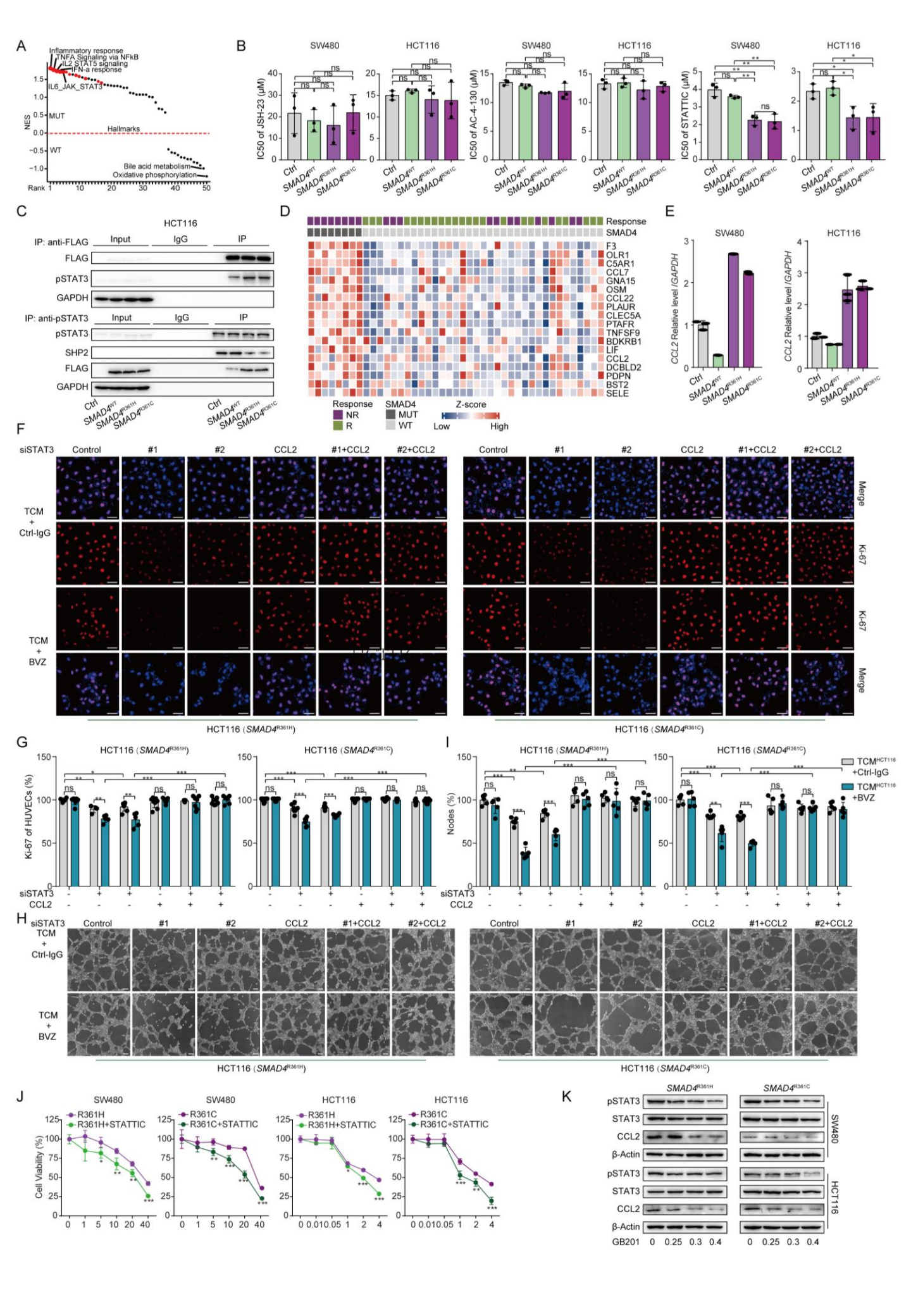
A
Inflammatory response
TNFA Signaling via NFkB
IL2 STAT5 signaling
IFN-a response
IL6_JAK_STAT3
MUT
Hallmarks
WT
Bile acid metabolism
Oxidative phosphorylation
NES
Rank
B
SW480
HCT116
IC50 of JSH-23 (μM)
IC50 of AC-4-130 (μM)
IC50 of STATTIC (μM)
Ctrl
SMAD4WT
SMAD4R361H
SMAD4R361C
C
HCT116
IP: anti-FLAG
IP: anti-pSTAT3
Input
IgG
IP
FLAG
pSTAT3
GAPDH
SHP2
D
Response
SMAD4
NR
R
MUT
WT
Z-score
Low
High
F3
OLR1
C5AR1
CCL7
GNA15
OSM
CCL22
PLAUR
CLEC5A
PTAFR
TNFSF9
BDKRB1
LIF
CCL2
DCBLD2
PDPN
BST2
SELE
E
CCL2 Relative level /GAPDH
F
siSTAT3
Control
#1
#2
CCL2
#1+CCL2
#2+CCL2
TCM + Ctrl-IgG
TCM + BVZ
Merge
Ki-67
HCT116 (SMAD4R361H)
HCT116 (SMAD4R361C)
G
Ki-67 of HUVECs (%)
I
Nodes (%)
TCMHCT116 +Ctrl-IgG
TCMHCT116 +BVZ
H
J
Cell Viability (%)
R361H
R361H+STATTIC
R361C
R361C+STATTIC
K
pSTAT3
STAT3
CCL2
β-Actin
GB201
0
0.25
0.3
0.4

FigureS11. *SMAD4*$^{R361H/C}$mutations induce resistance to BVZ therapy in CRC via the pSTAT3-CCL2 axis, related to Figure 6.
(A) Dot plot showing significantly enriched HALLMARK gene sets in CRLM with *SMAD4* mutation. **(B)** IC50 value of JSH-23 (NF-κB inhibitor), AC-4-130 (STAT5 inhibitor) and STATTIC (pSTAT3 inhibitor) in SW480 and HCT116 cells. **(C)** Co-IP assay shows a complex containing pSTAT3 and FLAG-SMAD4^{R361H}, SMAD4^{R361C}, or SHP2 in HCT116 cells. Top, FLAG antibody coprecipitating pSTAT3. Bottom, pSTAT3 antibody coprecipitating FLAG-SMAD4^{R361H}, SMAD4^{R361C}, or SHP2 protein. Input, protein expression in cell lysates detected by Western blot. IgG, negative control. IP, expression of compound coprecipitated by pSTAT3 or FLAG antibody. **(D)** Heatmap showing the DEGs in pre-treatment samples with versus without *SMAD4* mutation.The DEGs were identified using the limma method. The signicant DEGs (log2foldchange > 1 and P-value < 0.05) within the HALLMARK inflammatory response gene set are shown. **(E)** QPCR analysis of *CCL2* in SW480 and HCT116 cells with R361H/C mutation. **(F-I)** HCT116 cells with R361H/C mutations were transfected with siRNA of *STAT3* for 24h and replaced with fresh culture medium for 48h. Immunofluorescence staining for Ki-67 (red) and DAPI (blue) in HUVECs incubated with TCM collected from the indicated cells with *STAT3* silence, BVZ (0.25 mg/ml) and CCL2 protein (50 μg/ml). Representative immunofluorescence images **(F)** and the quantification **(G)** of MFI are shown (n=4~5). Scale bar, 100 μm; representative images **(H)** and quantification **(I)** of the formation of HUVECs tubules following incubation with TCM collected from the indicated cells with *STAT3* silence, and treatment with BVZ (0.25 mg/ml) and CCL2 protein (50 μg/ml) (n=4~5). Scale bar, 100 μm. **(J)** Cell viability of SW480 and HCT116 cells with R361H/C mutation exposed to 5-FU at the gradient concentrations, with or without combination with STATTIC. **(K)** Western blot analysis of pSTAT3 and CCL2 in SW480 and HCT116 cells with R361H/C mutations following treatment with GB201 at the gradient concentrations. Data are graphed as the mean ± SD; *, P < 0.05; **, P < 0.01; ***, P < 0.001; ns, nonsignificant, P > 0.05.

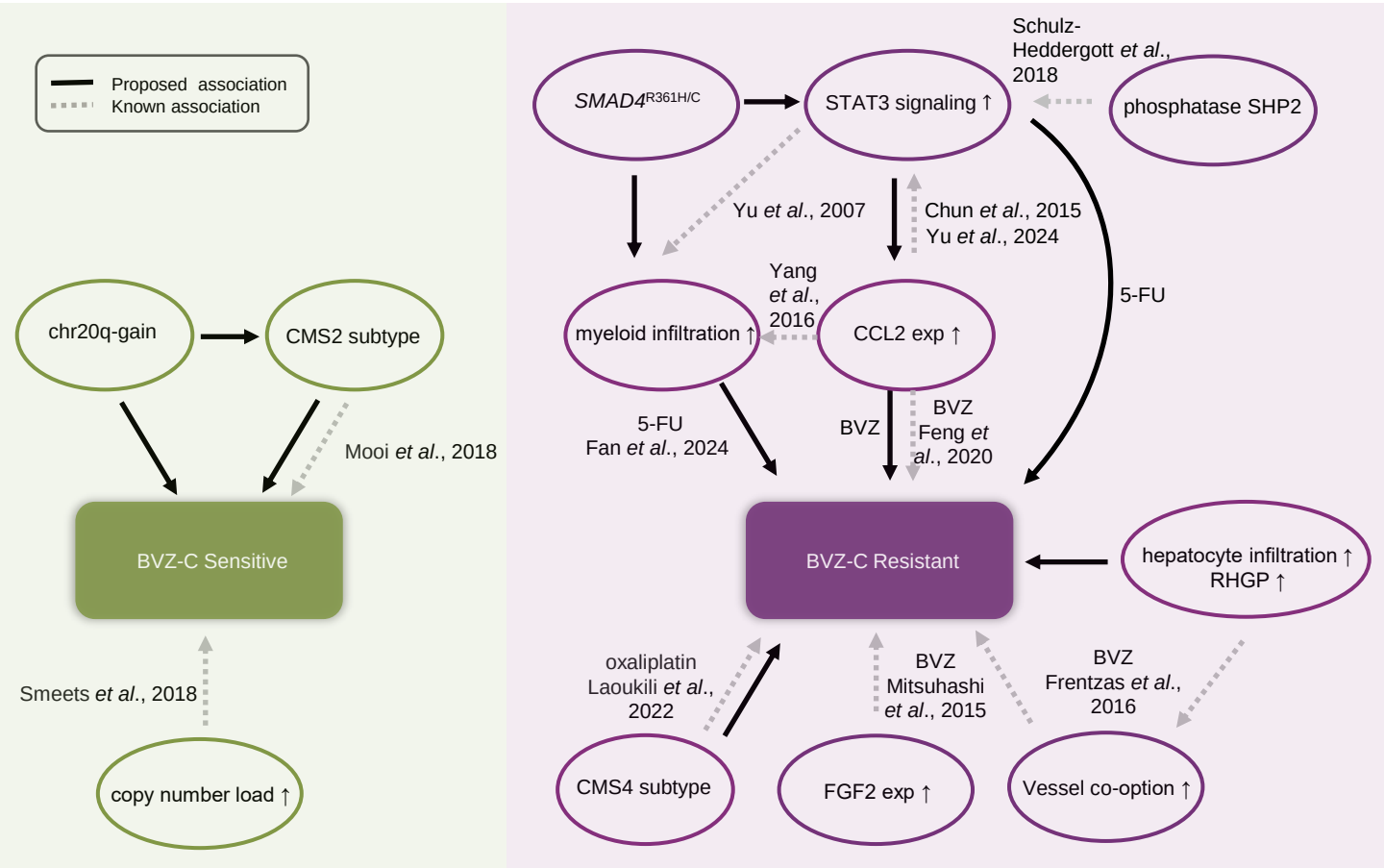

Figure S12. Summary representation of the known and newly identified molecular features linked to BVZ-C response in CRLM, related to Figure 6.

Previous papers reporting the associations are labelled. Features with black lines are the associations proposed in this study. Arrows directed upward within the circles indicate activated signaling, high expressed or increased number..